CHINESE OPTICS LETTERS

Vol. 22, No. 3 | March 2024

Microwave photonic sideband selector based on thin-film lithium niobate platform

Yuedi Ding (丁跃迪)[1,2,†], Chenglin Shang (尚成林)[3,†], Wenqi Yu (于文琦)[1,2], Xiang Ma (马 向)[1,2], Shaobo Li (李少波)[1,2], Cheng Zeng (曾 成)[3*], and Jinsong Xia (夏金松)[3**]

[1] 54th Institute, China Electronics Technology Group Corporation, Shijiazhuang 050011, China

[2] Hebei Key Laboratory of Photonic Information Technology and Application (PITA), Shijiazhuang 050011, China

[3] Wuhan National Laboratory for Optoelectronics, Huazhong University of Science and Technology, Wuhan 430074, China

[†]These authors contributed equally to this work.

*Corresponding author: zengchengwuli@hust.edu.cn

**Corresponding author: jsxia@hust.edu.cn

Received October 5, 2023 | Accepted November 29, 2023 | Posted Online March 25, 2024

We propose and demonstrate an integrated microwave photonic sideband selector based on the thin-film lithium niobate (TFLN) platform by integrating an electro-optic Mach–Zehnder modulator (MZM) and a thermo-optic tunable flat-top microring filter. The sideband selector has two functions: electro-optic modulation of wideband RF signal and sideband selection. The microwave photonic sideband selector supports processing RF signals up to 40 GHz, with undesired sidebands effectively suppressed by more than 25 dB. The demonstrated device shows great potential for TFLN integrated technology in microwave photonic applications, such as mixing and frequency measurement.

Keywords: lithium niobate; microwave photonics; sideband selector.

DOI: 10.3788/COL202422.031304

1. Introduction

Microwave photonics was proposed to utilize the advantages of photonics technology, including large bandwidth, flexible reconfiguration, and electromagnetic interference (EMI) immunity[1–3]. Up to now, microwave photonic technology has been verified and developed in discrete devices based on optical fiber and RF link cable, and it has shown significant progress. However, such microwave photonic systems are generally bulky in volume and lack stability. With the rapid development of photonic integration, integrating core optoelectronic devices onto the chip to form chip-scale microsystems is considered as a feasible technological route[4]. Currently, integrated microwave photonic signal processing microsystems have been explored on three main integrated optical material platforms: silicon-on-insulator (SOI)[5,6], silicon nitride (Si_3N_4)[7,8], and indium phosphide (InP)[9,10]. Each material exhibits obvious strengths and weaknesses. SOI offers excellent CMOS compatibility that is suitable for large-scale integration of passive devices. Si_3N_4 possesses ultralow waveguide transmission loss and a high third-order nonlinear coefficient, which makes it a promising platform for Kerr frequency combs. But both of them are poor materials for active devices. The InP platform can realize monolithic integration of active and passive devices. However, the system performance is limited by its relatively large transmission loss. In addition, they all face the challenge of achieving high-performance electro-optic devices. In recent years, thin-film lithium niobate (TFLN) has emerged as an attractive functional material platform due to its wide transparency window, high electro-optic coefficient, and high refractive index contrast[11–13]. Till now, TFLN monolithic electro-optic modulators have achieved unprecedented excellent performance in many aspects[14,15], such as high bandwidth (>100 GHz)[16], few-volt half-wave voltage[17], and low on-chip insertion loss (<0.5 dB). In addition, the low waveguide loss of TFLN allows the development of narrow bandwidth TFLN photonic signal processing units[18–20]. Thus, TFLN is a promising complementary platform for the development of integrated microwave photonics devices.

A typical microwave photonic signal processing system includes light sources, modulators, optical filters, and detectors. As essential electronic-optic conversion devices, the properties of modulators affect the performance of microwave photonic systems. For instance, the bandwidth of the modulator determines the upper limit of the working bandwidth of the system. The linearity of the modulator affects the dynamic range of the system. Optical filters are generally adopted to achieve sideband selection or suppression in the optical domain[21]. For example,

in a typical microwave frequency measurement system, the relationship of optical power and microwave frequency is established by measuring the output power change of optical filters[22]. In the microwave photonic mixing system, optical filters are used to suppress mixing spurs[23,24]. The performance of the filter affects the quality of sideband selection. In order to enhance the frequency selectivity and out-of-band suppression effect, tunable filters with high extinction ratio and near-rectangular filtering response are always required.

In this work, we report a microwave photonic sideband selector based on the TFLN platform. The device mainly consists of a wideband asymmetrical electro-optic Mach–Zehnder modulator (MZM) and a thermo-optic tunable flat-top microring filter with GHz bandwidth and high out-of-band suppression ratio. Due to the high performance of components of the microwave photonic sideband selector, it supports working bandwidth up to 40 GHz, with undesired sidebands effectively suppressed by more than 25 dB. The related design methods and principles have been reported by our research team previously[25–28]. The insertion loss of a packaged microwave photonic sideband selector is approximately 11 dB, occupying a volume of 35 mm × 10 mm × 5 mm. To the best of our knowledge, this is the first demonstration of microwave photonic sideband selector based on the TFLN platform. The potential applications of the demonstrated device include microwave photonic mixing and frequency measurement.

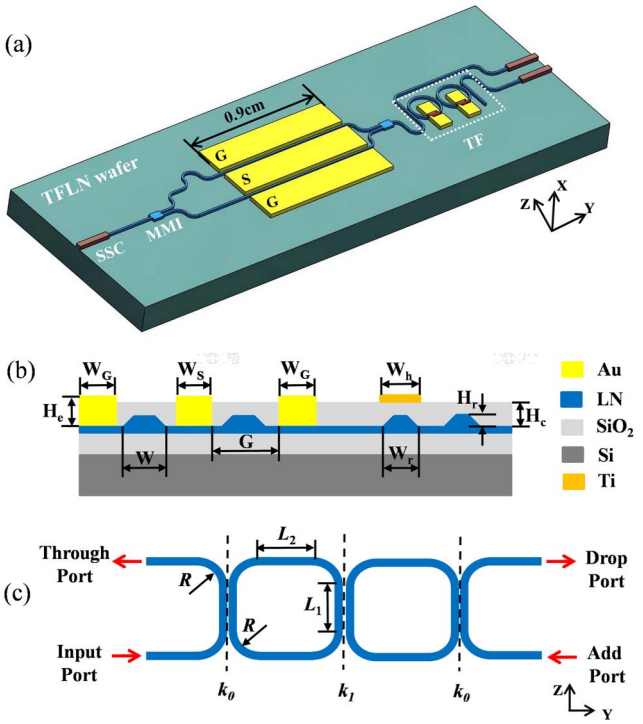

Fig. 1. (a) Schematic diagram of TFLN microwave photonic sideband selector. (The schematic is not drawn to scale.) (b) Cross-sectional view of the electro-optic modulation region and the thermo-optic tunable filter; (c) definition of design parameters of the microring filter.

2. Design and Simulation

The schematic diagram of the proposed TFLN microwave photonic sideband selector is shown in Fig. 1(a). The device is designed on the 500-nm-thick *X*-cut TFLN wafer. It consists of multimode interferometers (MMIs), spot-size converters (SSCs), an asymmetric electro-optic MZM, and a thermo-optic tunable flat-top microring filter. For the convenience of testing, an asymmetric MZM is adopted in the design. The electro-optic MZM is driven by a 0.9-cm-long ground–signal–ground (GSG) traveling-wave electrode working in a push–pull mode. The central wavelength of the passband of the filter is adjustable utilizing the thermo-optic effect of LN to select the target sideband generated by electro-optic modulation. In addition, spot-size converters are adopted for chip-to-fiber coupling. Two 50:50 MMIs are used as symmetrical optical power splitters and combiners.

The cross-sectional view of the electro-optic modulation region is shown in Fig. 1(b). By reasonably setting the electrode parameters, waveguide width, and etching depth, an excellent electro-optic performance can be achieved. The LN ridge waveguide has a width of $W = 1.5\,\mu m$, and the etching depth H_r is 260 nm. The electrode structure is optimized by the finite element method (FEM). The widths of signal and ground electrodes are designed as $W_S = 40\,\mu m$ and $W_G = 50\,\mu m$, respectively. The thickness of the electrode is $H_e = 1.2\,\mu m$. The electrode gap is designed to $G = 5\,\mu m$ by a finite difference eigenmode (FDE) solver. The cross-sectional view of the waveguide and the heater of the filter is shown in Fig. 1(b). The etching depth H_r of the LN ridge waveguide is 260 nm, and the width of the ridge waveguide W_r is 1.2 μm with a 70° sidewall angle of the cross section to ensure single-mode transmission. The width of the microheater Ti W_h is 2.5 μm. The top cladding thickness $H_c = 1\,\mu m$, to avoid introducing additional loss by the absorption of electrodes. Figure 1(c) shows the relevant design parameters of the microring filter. To achieve high out-of-band extinction ratio, narrow and flat-top passband simultaneously, coupling coefficients k_0 and k_1 are chosen to be 0.3 and 0.034, respectively. In this paper, the length of coupling region L_1 is set to 100 μm. The length of uncoupling region L_2 is set to 300 μm, and R is set to 130 μm. For a more detailed design process and methods of these integrated components included in this article, please refer to the references[25–28].

Figure 2(a) shows the operating principle of the proposed device. The target sideband generated by electro-optical modulation is purposefully filtered out by the tunable filter, while the optical carrier and the other sidebands are suppressed. The system simulations of the microwave photonic sideband selector were performed using integrated circuit solver Lumerical INTERCONNECT. The continuous-wave (CW) laser is used with a central frequency of 193.1 THz and output power of 10 dBm. The DC bias voltage is 1.37 V. The frequency of the input sine signal is 40 GHz, with normalized amplitude set to 0.5. The sample rate of the simulation is 0.16 THz, and the time window is 5.12×10^{-7} s. The simulation of dual sideband

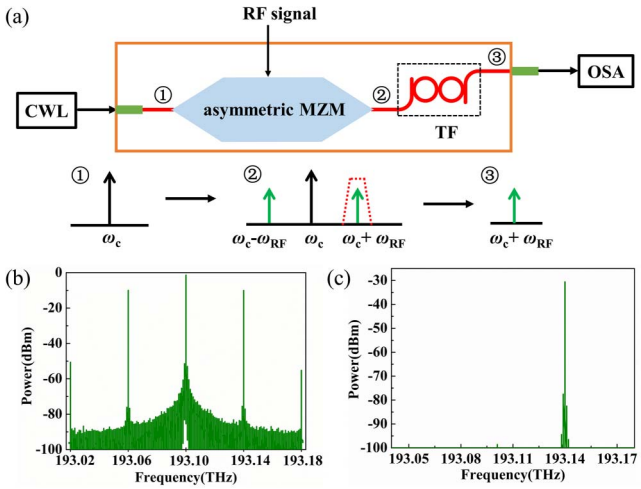

Fig. 2. (a) Working principle of the proposed microwave photonic sideband selector. CWL, continuous wave laser; MZM, Mach–Zehnder modulator; TF, tunable filter; OSA, optical spectrum analyzer. (b) Simulated dual sideband modulation; (c) simulated sideband selection.

modulation is performed first. As is shown in Fig. 2(b), modulation sidebands with an interval of 40 GHz on both sides of the optical carrier are symmetrically generated. The frequencies of two modulation sidebands are 193.06 and 193.14 THz, respectively. Then, the function of sideband selection is simulated by adding a rectangular filter with a sufficiently large extinction ratio. The central frequency of the filter is set to 193.14 THz. The 3 dB bandwidth is set to 4.8 GHz, which is based on the measurement values of the filter we previously reported[28]. As is shown in Fig. 2(c), the positive first-order modulation sideband is selected.

3. Device Fabrication and Measurement

All involved devices are fabricated on a commercial TFLN wafer (purchased from NANOLN). The patterns are defined using EBL (Vistec EPBG5000+) and inductively coupled plasma (ICP). Chrome is used as a hard mask for etching. The silicon dioxide cladding layer is deposited onto the LN layer by plasma-enhanced chemical vapor deposition (PECVD). The modulation electrodes and thermo-optic microheaters are deposited by electron-beam evaporation (EBE) and lift-off processes. The chemical mechanical polishing (CMP) treatment is carried out to make the end face of the spot-size converters smooth. The optical coupling between the LN waveguide and the polarization-maintaining fiber array (mode field diameter is 3.5 μm) is achieved by UV curing adhesive. For electrical packaging, a ceramic submount for the transmission connection of the RF signals is used. In order to minimize RF loss and reflection, a specific RF link is designed, including RF transmission lines mounted on ceramics to carry the driving signals from 1.85 mm coaxial connectors and from modulators to an off-chip matching resistor (38 Ω).

The electro-optic responses of the TFLN asymmetric MZM is characterized by using a vector network analyzer (Ceyear, 3672E). As is shown in Fig. 3(a), the measured electro-optic 3 dB bandwidth is about 50 GHz, which determines the upper limit of working bandwidth of the proposed device. A continuous tunable laser (Santec, TLS-510), an optical power meter (AQ2211, Yokogawa), and a programming computer constitute the wavelength scanning system to measure the optical transmission spectrum of the TFLN filter. As is shown in Fig. 3(b), the filter has a 3 dB bandwidth of about 4.8 GHz and an out-of-band rejection ratio of 33.48 dB. The free spectral range (FSR) is about 1.6 nm.

The image of the packaged microwave photonic sideband selector is shown in Fig. 4(a). The packaged device occupies a volume of 35 mm × 10 mm × 5 mm. We measured the optical transmission spectrum of microwave photonic sideband selector to verify the process technology level and determine whether integration has been achieved. As is shown in Fig. 4(b), the transmission spectrum of the sideband selector contains two kinds of periodic transmission spectrum and preserves characteristics of the asymmetric MZM and the microring filter. Figure 4(b) shows that the measured on-chip insertion loss of the packaged device is approximately 11 dB. The microwave photonic sideband selector exhibits an extinction ratio of 39 dB, which proves that the spectral ratio of the MMI is very close to 50:50 and verifies that the process technology level is relatively high. Taking into account the above measurement results, it is indicated that monolithic integration of a single MZM and filter has been achieved.

Finally, the function of sideband selection is evaluated. A sine signal at 40 GHz of 10 dBm is generated by the signal generator (Keysight, N51738) and sent into the microwave photonic sideband selector. The optical carrier with a central frequency of 193.10 THz with output power of 0 dBm is provided by a continuous tunable laser (Santec, TSL-510). The precision DC power supply (Keysight, B2901A) is used to adjust the central wavelengths of the filters. For the asymmetrical electro-optic MZM, the electro-optic modulation effect is similar to dual sideband modulation, with relatively low modulation efficiency. Figure 5(a) exhibits the electro-optic modulation optical spectra after the asymmetrical MZM. The positive and negative first-order sidebands and higher-order sidebands are generated. In the experiment, the target sideband is a positive first-order

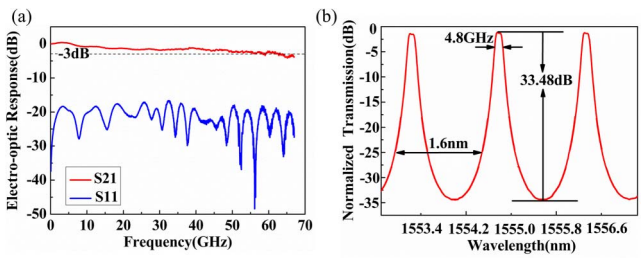

Fig. 3. (a) Normalized electro-optic responses of the TFLN asymmetric MZM; (b) measured bandpass filtering response of the TFLN filter.

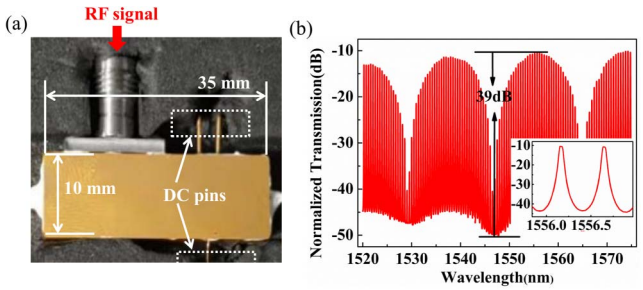

Fig. 4. (a) Image of the packaged microwave photonic sideband selector; (b) optical transmission spectrum of the microwave photonic sideband selector. The illustration is a partially enlarged view of the optical transmission spectrum of the microwave photonic sideband selector.

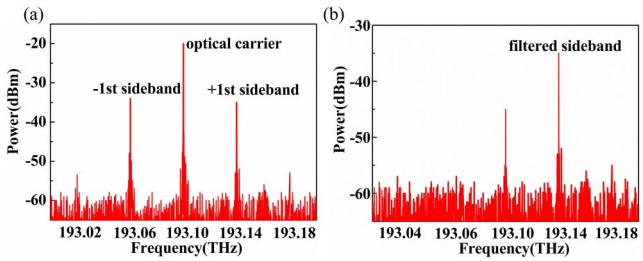

Fig. 5. (a) Measured optical spectra after asymmetrical MZM; (b) measured optical spectra of sideband selection of the demonstrated TFLN microwave photonic sideband selector.

sideband. Subsequently, the central frequency of the filter is adjusted to align with the positive first-order sideband. As shown in Fig. 5(b), the positive first-order sideband is filtered out, while the optical carrier and negative first-order sideband are suppressed by 25 dB.

4. Conclusions

In conclusion, we first propose and demonstrate a monolithic microwave photonic sideband selector based on the TFLN platform. The device consists of on-chip spot-size converters, an electro-optic MZM, and a thermo-optic flat-top tunable microring filter. It has achieved two functions: electro-optic modulation of a wideband RF signal and target sideband selection. The microwave sideband selector supports a working bandwidth up to 40 GHz, with undesired sidebands effectively suppressed by more than 25 dB. The packaged microwave photonic sideband selector exhibits a compact volume of 35 mm × 10 mm × 5 mm and low insertion loss of approximately 11 dB. The microwave photonic sideband selector can find its application in microwave photonic signal processing systems, such as microwave photonic mixing, frequency measurement, and microwave photonic receivers. Although the demonstrated microwave photonic sideband selector has shown the potential for developing integrated microwave photonics on the TFLN platform, its performance needs to be further improved in two aspects. The current device has the problem of insufficient suppression ratio of undesired sidebands. Thus, the extinction ratio of the filter needs to be further improved through cascading more microrings or adopting other structures. To achieve more flexible microwave photonic signal processing, reconfigurable filters need to be designed and implemented.

Acknowledgements

This work was supported by the National Key Research and Development Program of China (No. 2021YFB2800104) and the National Natural Science Foundation of China (Nos. 62175079 and 62205119). We thank the Center of Micro-Fabrication and Characterization (CMFC) of WNLO and the Center for Nanoscale Characterization & Devices (CNCD), WNLO of HUST for the facility support.

References

1. S. Pan and J. Yao, "Photonics-based broadband microwave measurement," J. Lightwave. Tech. **35**, 3498 (2016).
2. J. Yao, "Microwave photonics," J. Lightwave. Tech. **27**, 314 (2009).
3. B. H. Kolner and D. W. Dolfi, "Intermodulation distortion and compression in an integrated electrooptic modulator," Appl. Opt. **26**, 3676 (1987).
4. D. Marpaung, J. Yao, and J. Capmany, "Integrated microwave photonics," Nat. Photonics **13**, 80 (2019).
5. D. Thomson, A. Zilkie, J. E. Bowers, *et al.*, "Roadmap on silicon photonics," J. Optic. **18**, 073003 (2016).
6. W. Zhang and J. Yao, "Silicon-based integrated microwave photonics," IEEE J. Quant. Electron. **52**, 0600412 (2015).
7. C. G. Roeloffzen, L. Zhuang, C. Taddei, *et al.*, "Silicon nitride microwave photonic circuits," Opt. Express **21**, 22937 (2013).
8. D. J. Moss, R. Morandotti, A. L. Gaeta, *et al.*, "New CMOS-compatible platforms based on silicon nitride and Hydex for nonlinear optics," Nat. Photonics **7**, 597 (2013).
9. M. Smit, X. Leijtens, H. Ambrosius, *et al.*, "An introduction to InP-based generic integration technology," Semicond. Sci. Tech. **29**, 083001 (2014).
10. S. Jin, A. Bhardwaj, P. Herczfeld, *et al.*, "RF/photonic link-on-chip PIC," IEEE Photon. Technol. Lett. **24**, 1139 (2012).
11. C. Wang, M. Zhang, X. Chen, *et al.*, "Integrated lithium niobate electro-optic modulators operating at CMOS-compatible voltages," Nature **562**, 101 (2018).
12. Y. Liu, H. Li, J. Liu, *et al.*, "Low V_π thin-film lithium niobate modulator fabricated with photolithography," Opt. Express **29**, 6320 (2021).
13. M. He, M. Xu, Y. Ren, *et al.*, "High-performance hybrid silicon and lithium niobate Mach–Zehnder modulators for 100 Gbit s^{-1} and beyond," Nat. Photonics **13**, 359 (2019).
14. P. Kharel, C. Reimer, K. Luke, *et al.*, "Breaking voltage–bandwidth limits in integrated lithium niobate modulators using micro-structured electrodes," Optica **8**, 357 (2021).
15. M. Xu, M. He, H. Zhang, *et al.*, "High-performance coherent optical modulators based on thin-film lithium niobate platform," Nat. Commun. **11**, 3911 (2020).
16. F. Yang, X. Fang, X. Chen, *et al.*, "Monolithic thin film lithium niobate electro-optic modulator with over 110 GHz bandwidth," Chin. Opt. Lett. **20**, 022502 (2022).
17. X. Liu, B. Xiong, C. Sun, *et al.*, "Wideband thin-film lithium niobate modulator with low half-wave-voltage length product," Chin. Opt. Lett. **19**, 060016 (2021).
18. A. Prencipe, M. A. Baghban, and K. Gallo, "Tunable ultranarrowband grating filters in thin-film lithium niobate," ACS Photonics **8**, 2923 (2021).

19. D. Pohl, F. Kaufmann, M. R. Escalé, *et al.*, "Tunable Bragg grating filters and resonators in lithium niobate-on-insulator waveguides," in *CLEO: Science and Innovations* (2020), paper STu4J.5.
20. M. R. Escalé, D. Pohl, A. Sergeyev, *et al.*, "Extreme electro-optic tuning of Bragg mirrors integrated in lithium niobate nanowaveguides," Opt. Lett. **43**, 1515 (2018).
21. A. Mast, C. Middleton, S. Meredith, *et al.*, "Extending frequency and bandwidth through the use of agile, high dynamic range photonic converters," in *2012 IEEE Aerospace Conference* (2012), p. 1.
22. X. Zou, H. Chi, and J. Yao, "Microwave frequency measurement based on optical power monitoring using a complementary optical filter pair," IEEE Trans. Microw. Theor. Tech. **57**, 505 (2009).
23. Z. Tang and S. Pan, "Microwave photonic mixer with suppression of mixing spurs," in *2015 14th International Conference on Optical Communications and Networks (ICOCN)* (2015), p. 1.
24. Z. Tang, Y. Li, J. Yao, *et al.*, "Photonics-based microwave frequency mixing: methodology and applications," Laser. Photon. Rev. **14**, 1800350 (2020).
25. X. Wang, C. Shang, A. Pan, *et al.*, "Thin-film lithium niobate based dual-polarization IQ modulator for single-carrier 1.6 Tb/s transmission," in *Integrated Optics: Devices, Materials, and Technologies XXVI* (2022), p. 87.
26. C. Shang, A. Pan, C. Hu, *et al.*, "112 Gb/s PAM4 electro-optic modulator based on thin-film LN-on-insulator," in *Optoelectronic Devices and Integration* (2019), paper OW1B.3.
27. C. Hu, A. Pan, T. Li, *et al.*, "High-efficient coupler for thin-film lithium niobate waveguide devices," Opt. Express **29**, 5397 (2021).
28. Y. Ding, S. Tao, X. Wang, *et al.*, "Thermo-optic tunable optical filters with GHz-bandwidth and flat-top passband on thin film lithium niobate platform," Opt. Express **30**, 22135 (2022).